Transport properties of Bi nanowire arrays

Yu-Ming Lin,[a] Stephen B. Cronin,[b] Jackie Y. Ying,[c] and M. S. Dresselhaus[a),b),d)]
Massachusetts Institute of Technology, Cambridge, Massachusetts 02139-4307

Joseph P. Heremans
Delphi Automotive Systems Central Research and Development, Warren, Michigan 48090-9055

(Received 3 April 2000; accepted for publication 8 May 2000)

To explain various temperature-dependent resistivity measurements $[R(T)]$ on bismuth (Bi) nanowires as a function of wire diameter down to 7 nm, a semiclassical transport model is developed, which explicitly considers anisotropic and nonparabolic carriers in cylindrical wires, and the relative importance of various scattering processes. $R(T)$ of 40 nm Bi nanowires with various Te dopant concentrations is measured and interpreted within this theoretical framework. © *2000 American Institute of Physics.* [S0003-6951(00)03026-6]

Bi wires of sub-100 nm diameter have attracted much attention in theoretical and experimental studies because their small electron effective mass allows study of quantum-confinement effects at a relatively large diameter ($\sim$40 nm). Recently, Bi nanowire arrays with diameters of 5–200 nm have been fabricated by liquid-phase pressure injection,[1,2] vapor-phase deposition,[3] or electrochemical deposition,[4,5] and various transport measurements have been performed[2–10] to study classical and quantum finite-size effects. However, a quantitative explanation of these measurements has been very challenging due to the complex band structure and the additional scattering processes in Bi nanowires. In this letter, we present a transport model for cylindrical Bi wires, which explains the various features in the temperature-dependent resistance $R(T)$ of Bi nanowires. This theoretical framework is then extended to study the transport properties of Te-doped Bi nanowires.

Bi, as a semimetal, has an equal number of electrons and holes, each with highly anisotropic Fermi surfaces. Group VI and IV elements such as Te and Sn (or Pb), serve as *n*- and *p*-type dopants in Bi, respectively.[11,12] The transport properties of Bi nanowires are strongly dependent on the crystal orientation, the wire diameter d_w, and the dopant concentration. Bi nanowire arrays produced by pressure injection and vapor deposition methods are highly crystalline,[1,3] with the wire axes oriented along a common crystallographic direction, which is found to depend on d_w [see Fig. 1(a)]. By normalizing areas of the peaks in Fig. 1(a) to a bulk Bi standard, the major ($>$80%) crystal orientations of the wire axes in the 95 and 40 nm Bi nanowire arrays are, respectively, normal to the (202) and (012) lattice planes, which are denoted by $[10\bar{1}1]$ and $[01\bar{1}2]$ in the hexagonal lattice structure. In earlier studies,[9] a preferred axis orientation along the $[10\bar{1}1]$ direction was observed for Bi nanowires of large d_w (65 and 109 nm). Collectively, these observations suggest that most of the Bi nanowires are oriented along the $[10\bar{1}1]$ and $[01\bar{1}2]$ directions for $d_w \geqslant 60$ nm and $d_w \leqslant 50$ nm, respectively. We attribute the existence of more than one dominant orientation in the 52 nm Bi nanowires [see Fig. 1(a)] to the transitional behavior of *intermediate*-diameter nanowires as the preferential growth orientation shifts from $[10\bar{1}1]$ to $[01\bar{1}2]$ with decreasing d_w. The critical wire diameters d_c for the semimetal–semiconductor transition are predicted as 48.7 and 49.0 nm at 77 K for Bi nanowires oriented along $[10\bar{1}1]$ and $[01\bar{1}2]$, respectively.[13,14]

Systematic measurements of the T dependence of the resistance $R(T)$ for Bi nanowires (7–200 nm in d_w) synthesized by vapor deposition were reported,[3] showing a very different T dependence from that of bulk Bi, with $R(T)$ very sensitive to d_w [see Fig. 1(b)]. Here, a comparison of these experiments is made to a transport model for Bi nanowires,[13] which explicitly considers the circular wire boundary, anisotropic carrier pockets, and nonparabolic dispersion relations. The solid curves in Fig. 1(c) show the calculated $R(T)/R(300\,\mathrm{K})$ of 70 nm (semimetallic) and 36 nm (semiconducting) Bi nanowires, showing trends consistent with experiments in Fig. 1(b). In this model, additional scattering processes are considered for actual Bi nanowires, including wire-boundary and grain-boundary scattering, and ionized impurity scattering, due to uncontrolled charged impurities. Evidence for boundary scattering due to finite-amplitude electron wave functions at the wire boundary comes from magnetoresistance measurements.[3,9,10] Evidence for uncontrolled dopants comes from the weak T dependence of $R(T)$ at low T, indicating a finite carrier density. The reduction in the total carrier mobility μ_{tot} by various scattering processes is handled by Matthiessen's rule:[15]

$$\frac{1}{\mu_{\mathrm{tot}}(T)} = \frac{1}{\mu_{\mathrm{bulk}}(T)} + \frac{1}{\mu_{\mathrm{bound}}} + \frac{1}{\mu_{\mathrm{imp}}(T)}, \tag{1}$$

where μ_{bulk} is the carrier mobility in bulk crystalline Bi, and the terms $\mu_{\mathrm{bound}}^{-1}$ and μ_{imp}^{-1}, respectively, account for boundary scattering and charged impurity scattering. The T dependence of $\mu_{\mathrm{bulk}}(T)$ is mainly due to electron–phonon scattering,[16] while μ_{bound} is assumed to be T independent. Since the carriers contributing to the transport phenomena of undoped Bi nanowires are usually located near the first subband edge, they can be well described by a parabolic dispersion relation,[14] with $\mu_{\mathrm{imp}} \sim T^{3/2}$. The curve for the 36 nm Bi

[a)]Department of Electrical Engineering and Computer Science.
[b)]Department of Physics.
[c)]Department of Chemical Engineering.
[d)]Electronic mail: millie@mgm.mit.edu

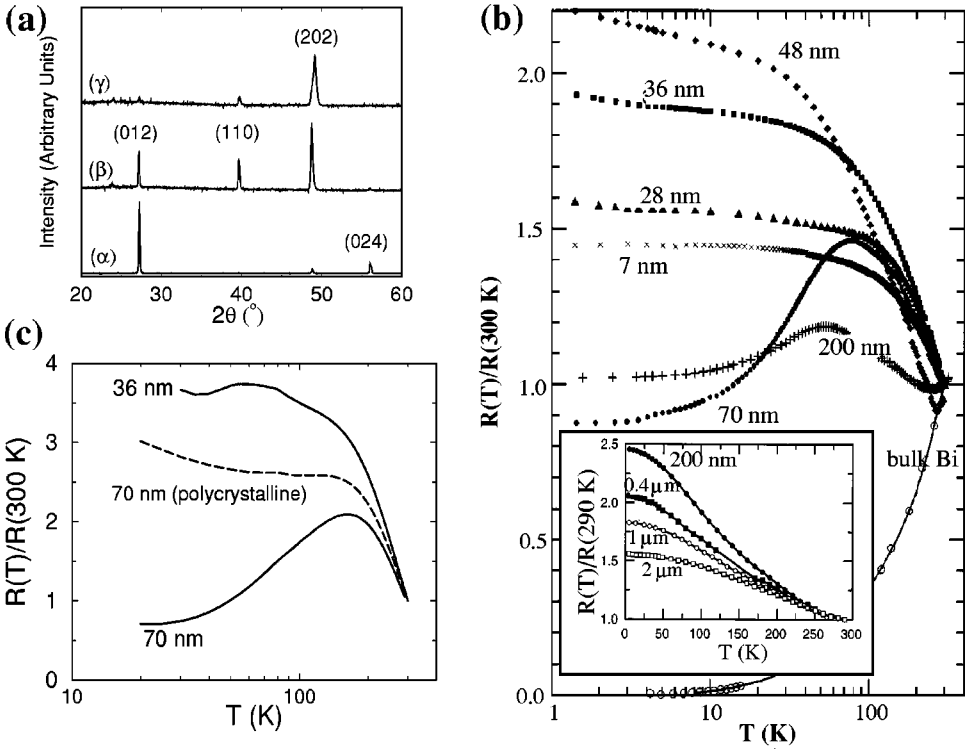

FIG. 1. (a) XRD patterns of Bi nanowire arrays with d_w of: (α) 40 nm, (β) 52 nm, and (γ) 95 nm. (b) Measured T dependence of the resistance for Bi nanowires of various d_w by Heremans *et al.* (Ref. 3) and Hong *et al.* (Ref. 6) (inset). (c) Calculated $R(T)/R(300\,\mathrm{K})$ of 36 and 70 nm Bi nanowires. The dashed curve refers to a 70 nm polycrystalline wire with increased boundary scattering.

nanowires in Fig. 1(c) is fitted by $\mu_{\mathrm{bound}}=33\,\mathrm{m^2\,V^{-1}\,s^{-1}}$ and $\mu_{\mathrm{imp}}=0.2\times T^{3/2}\,\mathrm{m^2\,V^{-1}\,s^{-1}}$, and the uncontrolled impurity contribution is fitted to $N_{\mathrm{imp}}\simeq 5\times 10^{16}\,\mathrm{cm^{-3}}$. The data (solid curve) for the 70 nm Bi nanowires are fitted by $\mu_{\mathrm{bound}}\simeq 50\,\mathrm{m^2\,V^{-1}\,s^{-1}}$ and $\mu_{\mathrm{imp}}\simeq 1.0\times T^{3/2}\,\mathrm{m^2\,V^{-1}\,s^{-1}}$. Since 70 nm Bi nanowires are semimetallic, the carrier density contribution due to N_{imp} can be neglected. The smaller value of $\mu_{\mathrm{bound}}^{-1}$ for the 70 nm wires is attributed to a smaller fraction of atoms on the nanowire surface for 70 nm relative to 36 nm wires. The T dependence of $R(T)$ of Bi nanowires, which is strongly affected by the crystal quality, is expressed by the value of μ_{bound}. Instead of a nonmonotonic behavior for semimetallic Bi nanowires, as shown in Fig. 1(b), $R(T)$ is predicted to show a monotonic T dependence at a higher defect level. The dashed curve in Fig. 1(c) shows the calculated $R(T)/R(300\,\mathrm{K})$ for 70 nm wires with increased boundary scattering ($\mu_{\mathrm{bound}}\simeq 6\,\mathrm{m^2\,V^{-1}\,s^{-1}}$), exhibiting a monotonic T dependence similar to that of polycrystalline Bi nanowires [$\geqslant 200$ nm, see the inset to Fig. 1(b)].

The same transport model has also been extended to describe the transport properties of Te-doped Bi nanowires. In this study, 40 nm Bi nanowires with various Te concentrations (0–0.15 at. %) were prepared by a pressure injection process.[17] XRD studies show that the crystal structure and the preferred axis orientation of these nanowires are not affected by small amounts of Te dopants.[14,17] Since Bi has a large dielectric constant (~ 100) and very small electron effective masses, Te donors in Bi have a very small ionization energy, and the freeze-out temperature of Te atoms in 40 nm Bi nanowires is about 2 K.[14] Therefore, all the donor atoms are likely ionized in our 40 nm Bi nanowires for $4\leqslant T\leqslant 300$ K. Figure 2 shows the measured $R(T)/R(270\,\mathrm{K})$ of 40 nm Bi nanowires with Te concentrations based on the Bi/Te atom ratio that was introduced to form the alloy prior to the nanowire synthesis. The actual Te concentration is smaller than the nominal concentration due to the likely segregation of some Te atoms to the wire boundary during alloy solidification.[10] For discussion purposes, we assume that $\delta=10\%$ of the Te dopant in the alloy melt is present in the final nanowire product, so that 0.025, 0.075, and 0.15 at. % Te-doped Bi alloys give rise to donor concentrations N_d of 6.67×10^{17}, 2.0×10^{18}, and $4.0\times 10^{18}\,\mathrm{cm^{-3}}$ in the respective resulting nanowires. Based on the measured $R(T)$ in Fig. 2 and the calculated T-dependent carrier density, the T dependence of the average mobility μ_{avg} of these Te-doped Bi nanowires is obtained, shown as $\mu_{\mathrm{avg}}^{-1}(T)/\mu_{\mathrm{avg}}^{-1}(270\,\mathrm{K})$ in Fig. 3. Analogous to Eq. (1), μ_{avg}^{-1} of Te-doped Bi nanowires can be related to the various scattering processes by $\mu_{\mathrm{doped}}^{-1}(T)=\mu_{\mathrm{undoped}}^{-1}(T)+\mu_{\mathrm{imp}}^{-1}(T)+\mu_{\mathrm{defect}}^{-1}$, where μ_{undoped} is the average mobility of the undoped Bi nanowires of the same diameter, and μ_{imp}^{-1} and $\mu_{\mathrm{defect}}^{-1}$ are associated with the increased ionized impurity scattering and the expected higher

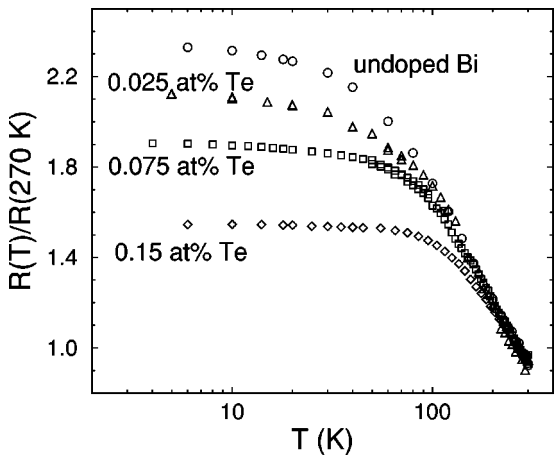

FIG. 2. Measured $R(T)/R(270\,\mathrm{K})$ for 40-nm-undoped and Te-doped Bi nanowires at different doping levels.

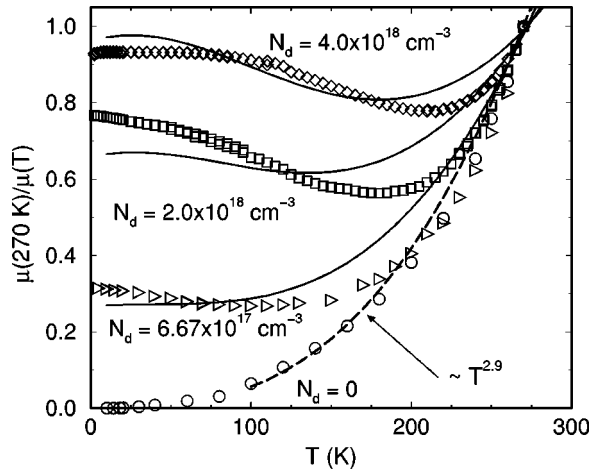

FIG. 3. Calculated T dependence of μ_{avg}^{-1} for 40-nm-undoped and Te-doped Bi nanowires of different N_d. The dashed and solid curves, respectively, are fitting curves corresponding to undoped and Te-doped Bi nanowires.

defect level in Te-doped Bi nanowires, respectively. At high $T\,(>200\,\text{K})$, the three Te-doped samples in Fig. 3 exhibit a similar T dependence to that of the undoped sample, indicating that $\mu_{\text{undoped}}^{-1}$ is the major contributor to μ_{doped}^{-1}. The average mobility of undoped Bi nanowires can be well fitted by a $\mu_{\text{undoped}} \sim T^{-2.9}$ dependence for $T>100\,\text{K}$, as shown by the dashed line in Fig. 3, consistent with the predominant electron–phonon scattering at high T. For most materials, electron–phonon scattering yields a T-dependent mobility[18] $\mu_{\text{phonon}} \propto m^{*-5/2} T^{-3/2} \propto T^{-1.5}$. However, μ_{phonon} of Bi has a stronger T dependence than $T^{-1.5}$ because the effective mass m^* of Bi increases with T.[16] The term μ_{defect}^{-1} is essentially T independent as is also neutral impurity scattering, while μ_{imp}^{-1} generally increases with decreasing T. Since $\mu_{\text{undoped}}^{-1}$ and $\mu_{\text{imp}}^{-1}+\mu_{\text{defect}}^{-1}$ are dominant contributors at high and low T, respectively, a minimum in μ_{doped}^{-1} is observed for Te-doped Bi nanowire arrays.

However, the $T^{-3/2}$ dependence generally expected[18] for μ_{imp}^{-1} cannot account for the much weaker T dependence observed in Te-doped Bi nanowires in Fig. 3 at low T. The ionized impurity scattering time is given by $\tau_{\text{imp}} \propto m^{*2} v^3$, where v is the carrier group velocity.[18] Since the L-point electrons have a nonparabolic dispersion relation, μ_{imp} for Bi nanowires has a different T dependence from that of materials with parabolic dispersion relations, and v along the wire axis (z direction) for electrons in the (n,m) subband is calculated as[14]

$$v_{nm}(k) = \frac{\partial E_{nm}}{\hbar\,\partial k} = \sqrt{\frac{2E_{gL}}{\tilde{m}_z}} \left(1 + \frac{\gamma_{nm}^2 \tilde{m}_z E_{gL}}{2\hbar^2 k^2}\right)^{-1/2}, \qquad (2)$$

where $E_{nm}(k)$ is the dispersion relation of the (n,m) subband, E_{gL} is the L-point band gap of bulk Bi, and $\tilde{m}_z = (\hat{z} \cdot \mathbf{m} \cdot \hat{z})$ is the transport effective mass along the wire. Here, $\mathbf{m}$ is the electron band-edge effective-mass tensor and $\gamma_{nm} = \sqrt{1+4\tilde{\varepsilon}_{nm}/E_{gL}}$ in which $\tilde{\varepsilon}_{nm}$ is the subband edge energy ignoring nonparabolic effects.[13] In Bi nanowires, the Te dopants raise E_F into the conduction band, and the group velocity of electrons responsible for the transport properties is approximately independent of energy, since $v \simeq \sqrt{2E_{gL}/\tilde{m}_z}$. Because of the T dependence of E_{gL} and $\tilde{m}_z$,[16] μ_{imp} is essentially T independent below 80 K, but increases approximately linearly with increasing T above 80 K. Therefore, we write μ_{doped}^{-1} as $\mu_{\text{doped}}^{-1} \simeq a T^{2.9} + b\,\eta(T)$, where $\eta(T) \simeq m^*(T)^{1/2} E_{gL}(T)^{-2/3}$ is an approximate T dependence of $\mu_{\text{imp}}^{-1}+\mu_{\text{defect}}^{-1}$. The ratio $\beta \equiv b/a$ expresses the importance of ionized impurity scattering relative to electron–phonon scattering. The data points in Fig. 3 are fitted by the solid curves, and a β ratio of 1.0:3.3:6.5 is found for Bi nanowires of $N_d = 6.67\times10^{17}$, 2.0×10^{18}, and $4.0\times10^{18}\,\text{cm}^{-3}$, respectively, indicating that μ_{imp}^{-1} is approximately proportional to N_d. In addition, the dependence $\beta \propto N_d$ is essentially independent of δ for small variation of δ.

In summary, we report here a transport model for Bi nanowires, which explains the measured $R(T)$ in both semimetallic and semiconducting nanowires. $R(T)$ depends on d_w, the Te dopant concentration, and on boundary, static defect, charged impurity, and electron–phonon scattering processes. This transport model not only accounts for various features in the measured $R(T)$ of Bi nanowires reported earlier[3–6,8,10] and in current experimental results for Te-doped Bi nanowires, but also provides a theoretical framework for future transport studies on this unique system.

The authors thank Dr. G. Dresselhaus, Professor G. Chen, and O. Rabin for valuable discussions. The support from MURI Subcontract No. 0205-G-7A114-01, NSF Grant No. DMR-98-04734, and U.S. Navy Contract No. N00167-92-K005 is gratefully acknowledged.

[1] Z. Zhang, D. Gekhtman, M. S. Dresselhaus, and J. Y. Ying, Chem. Mater. **11**, 1659 (1999).
[2] T. E. Huber, M. J. Graf, and C. A. Foss, Jr., *Proceedings of the 18th International Conference on Thermoelectrics*, Baltimore, MD (IEEE, Piscataway, NJ, 1999), p. 558.
[3] J. Heremans, C. M. Thrush, Y.-M. Lin, S. Cronin, Z. Zhang, M. S. Dresselhaus, and J. F. Mansfield, Phys. Rev. B **61**, 2921 (2000).
[4] K. Liu, C. L. Chien, P. C. Searson, and Y. Z. Kui, Appl. Phys. Lett. **73**, 1436 (1998).
[5] L. Piraux, S. Dubois, J. L. Duvail, A. Radulescu, S. Demoustier-Champagne, E. Ferain, and R. Legras, J. Mater. Res. **14**, 3042 (1999).
[6] K. Hong, F. Y. Yang, K. Liu, D. H. Reich, P. C. Searson, and C. L. Chien, J. Appl. Phys. **85**, 6184 (1999).
[7] J. Heremans, C. M. Thrush, Z. Zhang, X. Sun, M. S. Dresselhaus, J. Y. Ying, and D. T. Morelli, Phys. Rev. B **58**, R10091 (1998).
[8] K. Liu, C. L. Chien, and P. C. Searson, Phys. Rev. B **58**, 14681 (1998).
[9] Z. Zhang, X. Sun, M. S. Dresselhaus, J. Y. Ying, and J. Heremans, Appl. Phys. Lett. **73**, 1589 (1998).
[10] Z. Zhang, X. Sun, M. S. Dresselhaus, J. Y. Ying, and J. Heremans, Phys. Rev. B **61**, 4850 (2000).
[11] J. M. Noothoven Van Goor, Philips Res. Rep. **4**, 1 (1971).
[12] J. Heremans, D. T. Morelli, D. L. Partin, C. H. Olk, C. M. Thrush, and T. A. Perry, Phys. Rev. B **38**, 10280 (1988).
[13] Y.-M. Lin, X. Sun, and M. S. Dresselhaus, Phys. Rev. B (in press).
[14] Y.-M. Lin, Master's thesis, Massachusetts Institute of Technology (2000).
[15] N. W. Ashcroft and N. D. Mermin, *Solid State Physics* (Holt, Rinehart and Winston, New York, 1976), Chap. 16.
[16] M. P. Vecchi and M. S. Dresselhaus, Phys. Rev. B **10**, 771 (1974).
[17] Y.-M. Lin, X. Sun, S. Cronin, Z. Zhang, J. Y. Ying, and M. S. Dresselhaus, Mater. Res. Soc. Symp. Proc. **582** (in press).
[18] H. Brooks, Adv. Electron. Electron Phys. **7**, 158 (1955).